Available online at www.sciencedirect.com
SCIENCE DIRECT®
Journal of Sound and Vibration 292 (2006) 626–644
JOURNAL OF SOUND AND VIBRATION
www.elsevier.com/locate/jsvi

Free vibration response of two-dimensional magneto-electro-elastic laminated plates

Fernando Ramirez[a,*], Paul R. Heyliger[a], Ernian Pan[b]

[a]*Department of Civil Engineering, Colorado State University, Fort Collins, CO 80523, USA*
[b]*Department of Civil Engineering, University of Akron, Akron, OH 44325, USA*

Received 25 October 2004; received in revised form 20 May 2005; accepted 20 August 2005
Available online 21 October 2005

Abstract

An approximate solution for the free vibration problem of two-dimensional magneto-electro-elastic laminates is presented to determine their fundamental behavior. The laminates are composed of linear homogeneous elastic, piezoelectric, or magnetostrictive layers with perfect bonding between each interface. The solution for the elastic displacements, electric potential, and magnetic potential is obtained by combining a discrete layer approach with the Ritz method. The model developed here is not dependent on specific boundary conditions, and it is presented as an alternative to the exact or analytical approaches which are limited to a very specific set of edge conditions. The natural frequencies and through-thickness modal behavior are computed for simply supported and cantilever laminates. Solutions for the simply supported case are compared with the known exact solution for piezoelectric laminates, and excellent agreement is obtained. The present approach is also validated by comparing the natural frequencies of a two-layer cantilever plate with known analytical solution and with results obtained using commercial finite element software.

1. Introduction

Magneto-electro-elastic laminates show significant interactions between the elastic, electric, and magnetic fields due to the coupled nature of the constitutive equations. These laminates have direct application in sensing and actuating devices, such as damping and control of vibrations in structures. There have been several studies on the electric and mechanical behavior of piezoelectric laminates. Lee [1–4] published a series of papers incorporating the piezoelectric effect into the classical laminate theory. Tzou and Gadre [5] presented the dynamic equations for generalized multi-layered thin shells based on Love's theory and Hamilton's principle. More recently, Heyliger [6] and Heyliger and Brooks [7] presented an exact solution for the static behavior of laminated piezoelectric plates with simple supports. Heyliger and Brooks [8] also obtained the exact solution for the free vibration behavior of piezoelectric plates in cylindrical bending, by extending the free vibration solution of purely elastic simply supported plates to the corresponding piezoelectric case.

*Corresponding author. Tel.: +1 970 4912801.
E-mail address: framirez@engr.colostate.edu (F. Ramirez).

0022-460X/$ - see front matter © 2005 Elsevier Ltd. All rights reserved.
doi:10.1016/j.jsv.2005.08.004

Research on the behavior of magneto-electro-elastic laminates is relatively recent. Problems involving magneto-electro-elastic media have been considered by Harshe [9], Nan [10], and Benveniste [11] by developing expressions to determine the effective magnetoelectric effect in composites having piezoelectric and magnetostrictive phases. The exact closed-form solution for three-dimensional simply supported magneto-electro-elastic laminates was presented by Pan [12] based on the quasi-Stroh formalism and the propagator matrix method. Later, Pan and Heyliger [13,14] extended that solution to the corresponding free vibration problem, and to the static cylindrical bending of magneto-electro-elastic laminates. An approximate solution based on a discrete layer model was also obtained by Heyliger and Pan [15] and Heyliger et al. [16] for the cases of two- and three-dimensional magneto-electro-elastic laminates. More recently, Jiang and Ding [17] presented an analytical solution for the study of beams, Lage et al. [18] developed a layerwise mixed finite element model for plates, Buchanan [19] published a comparison between layered and multiphase models for the static and dynamic analysis of magneto-electro-elastic plates, Latheswary et al. [20] studied the dynamic response of moderately thick composite plates.

In this study, the governing equations of motion for two-dimensional linear magneto-electro-elastic laminates are solved using a discrete layer approximate model. Approximations for the three displacements and electric and magnetic potentials are constructed for each homogeneous layer such that the dependence on the in-plane directions and that on the thickness direction of the laminated plate can be separated. This separation allows for breaks in the gradients of the three displacement components and the two potentials across a dissimilar material interface. The free vibration behavior of a single homogeneous piezoelectric layer is studied first to check the present formulation with the known exact solution. The present approach is also validated by comparing the natural frequencies and mode shapes of a two-layer PZT-5A/graphite-epoxy cantilever plate with the analytical solution presented by Vel et al. [21], and with several finite element models. Finally, the natural frequencies, through-thickness modes shapes, and the influence of the piezoelectric and piezomagnetic coefficients on the natural frequencies of a two-layer $BaTiO_3/CoFe_2O_4$ cantilever plate are analyzed.

2. Theory

2.1. Geometry

Laminates are considered with the z-axis out of the laminate plane and the x- and y-axes are the corresponding in-plane axes of the laminate. This is shown in Fig. 1. The laminates are considered to be either very thin or infinitely long in the y-direction and are composed of an arbitrary number of elastic, piezoelectric, or magnetostrictive layers. The laminate has dimensions L_x in the x-direction and has total thickness H, with individual layer thicknesses h_1, h_2, and so on. Layer 1 is the bottom layer of the laminate and layer n is the top layer.

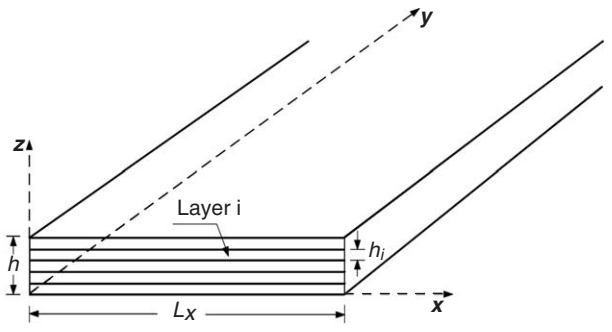

Fig. 1. Laminate geometry.

2.2. Governing equations

Magneto-electro-elastic laminates possess coupled field behavior between the elastic, electric, and magnetic field variables. For an anisotropic and linearly magneto-electro-elastic solid, the coupled constitutive relation for each layer can be written as [9]

$$\sigma_i = C_{ik}\gamma_k - e_{ki}E_k - q_{ki}H_k, \tag{1}$$

$$D_i = e_{ik}\gamma_k + \varepsilon_{ik}E_k + d_{ik}H_k, \tag{2}$$

$$B_i = q_{ik}\gamma_k + d_{ik}E_k + \mu_{ik}H_k. \tag{3}$$

Here Eqs. (1)–(3) describe the stress, electric displacement, and magnetic flux fields, respectively, and σ_i, D_i, and B_i denote the components of stress, electric displacement, and magnetic flux. The symbols C_{ij}, ε_{ij}, and μ_{ij} are the components of elastic stiffness, and the dielectric and magnetic permittivities; γ_k, E_k, and H_k denote the components of linear strain, electric field, and magnetic field; and e_{ij}, q_{ij}, and d_{ij} are the piezoelectric, piezomagnetic, and magnetoelectric coefficients. The standard engineering contraction in indices has been used here for the elastic variables (i.e., $\gamma_4 = \gamma_{23}$, etc.). The nonzero terms for the transversely isotropic material property tensors expressed in matrix form are shown in Appendix A, and the specific values for the different material properties are given in Table 1 [12,21,22].

Table 1
Material properties

Parameter	$CoFe_2O_4$	$BaTiO_3$	PZT-5A	PZT-4	Graphite-epoxy
C_{11} (GPa)	286.0	166.0	99.201	138.499	183.443
C_{22}	286.0	166.0	99.201	138.499	11.662
C_{33}	269.5	162.0	86.856	114.745	11.662
C_{13}	170.5	78.0	50.778	73.643	4.363
C_{23}	170.5	78.0	50.778	73.643	3.918
C_{12}	173.0	77.0	54.016	77.371	4.363
C_{44}	45.3	43.0	21.1	25.6	2.870
C_{55}	45.3	43.0	21.1	25.6	7.170
C_{66}	56.5	44.5	22.6	30.6	7.170
e_{31} (C/m^2)	0.0	−4.4	−7.209	−5.2	0.0
e_{32}	0.0	−4.4	−7.209	−5.2	0.0
e_{33}	0.0	18.6	15.118	15.08	0.0
e_{24}	0.0	11.6	12.322	12.72	0.0
e_{15}	0.0	11.6	12.322	12.72	0.0
q_{31} (N/Am)	580.3	0.0	0.0	0.0	0.0
q_{32}	580.3	0.0	0.0	0.0	0.0
q_{33}	699.7	0.0	0.0	0.0	0.0
q_{24}	550.0	0.0	0.0	0.0	0.0
q_{15}	550.0	0.0	0.0	0.0	0.0
ε_{11} ($10^{-9}C^2/Nm^2$)	0.080	11.2	1.53	1.306	1.53
ε_{22}	0.080	11.2	1.53	1.306	1.53
ε_{33}	0.093	12.6	1.5	1.115	1.53
$d_{11} = d_{22} = d_{33}$	0.0	0.0	0.0	0.0	0.0
μ_{11} ($10^{-6}Ns^2/C^22$)	−590.0	5.0	5.0	5.0	5.0
μ_{22}	−590.0	5.0	5.0	5.0	5.0
μ_{33}	157.0	10.0	10.0	10.0	10.0
ρ (kg/m^3)	5300.0	5800.0	7750.0	7600.0	1590.0

The components of strain, electric field, and magnetic field are related to the displacement field u_i, and the electric and magnetic potentials ϕ and ψ by the relations

$$\gamma_{ij} = \frac{1}{2}\left(\frac{\partial u_i}{\partial x_j} + \frac{\partial u_j}{\partial x_i}\right), \tag{4}$$

$$E_i = -\phi_{,i}, \tag{5}$$

$$H_i = -\psi_{,i}. \tag{6}$$

In the case of free vibration, the absence of body force, free charge density, and free current density are assumed. Under these conditions, the equations of motion can then be written as

$$\sigma_{ij,j} = \rho u_{i,tt}, \tag{7}$$

$$D_{i,i} = 0, \tag{8}$$

$$B_{i,i} = 0. \tag{9}$$

2.3. Variational formulation

Following the standard variational method of approximation (see Ref. [23]), we multiply each of the three governing equations by the first variation of the displacements, electric and magnetic potential, respectively, we then integrate the result over the volume of the plate, which is the domain bounding the magneto-electro-elastic medium, and set the result equal to zero, resulting in

$$\int_V \delta u_i(\sigma_{ij,j} - \rho u_{i,tt})\,\mathrm{d}V = 0, \tag{10}$$

$$\int_V \delta\phi(D_{i,i})\,\mathrm{d}V = 0, \tag{11}$$

$$\int_V \delta\psi(B_{i,i})\,\mathrm{d}V = 0. \tag{12}$$

Integrating each of these equations by parts and applying the divergence theorem yields the final weak form of the governing equations.

$$0 = \int_V (\sigma_{ij}\delta\gamma_{ij} + \delta u_i \rho u_{i,tt})\,\mathrm{d}V - \oint_S \sigma_{ij} n_j \delta u_i\,\mathrm{d}S, \tag{13}$$

$$0 = \int_V D_j \delta\phi_{,j}\,\mathrm{d}V - \oint_S D_j n_j \delta\phi\,\mathrm{d}S, \tag{14}$$

$$0 = \int_V B_j \delta\psi_{,j}\,\mathrm{d}V - \oint_S B_j n_j \delta\psi\,\mathrm{d}S. \tag{15}$$

Substituting the governing constitutive equations into final weak form yields

$$\begin{aligned} 0 = \int_V \Bigg\{ & \left[C_{11}\frac{\partial u}{\partial x} + C_{13}\frac{\partial w}{\partial z} + C_{14}\frac{\partial v}{\partial z} + C_{16}\frac{\partial v}{\partial x} + e_{11}\frac{\partial \phi}{\partial x} + e_{31}\frac{\partial \phi}{\partial z} + q_{11}\frac{\partial \psi}{\partial x} + q_{31}\frac{\partial \psi}{\partial z}\right]\frac{\partial \delta u}{\partial x} \\ & + \left[C_{12}\frac{\partial u}{\partial x} + C_{23}\frac{\partial w}{\partial z} + C_{24}\frac{\partial v}{\partial z} + C_{26}\frac{\partial v}{\partial x} + e_{12}\frac{\partial \phi}{\partial x} + e_{32}\frac{\partial \phi}{\partial z} + q_{12}\frac{\partial \psi}{\partial x} + q_{32}\frac{\partial \psi}{\partial z}\right]\frac{\partial \delta v}{\partial y} \\ & + \left[C_{13}\frac{\partial u}{\partial x} + C_{33}\frac{\partial w}{\partial z} + C_{36}\frac{\partial v}{\partial x} + e_{33}\frac{\partial \phi}{\partial z} + q_{33}\frac{\partial \psi}{\partial z}\right]\frac{\partial \delta w}{\partial z} \end{aligned}$$

$$+\left[C_{14}\frac{\partial u}{\partial x}+C_{44}\frac{\partial v}{\partial z}+C_{45}\left(\frac{\partial u}{\partial z}+\frac{\partial w}{\partial x}\right)+e_{14}\frac{\partial \phi}{\partial x}+q_{14}\frac{\partial \psi}{\partial x}\right]\frac{\partial \delta v}{\partial z}$$
$$+\left[C_{45}\frac{\partial v}{\partial z}+C_{55}\left(\frac{\partial u}{\partial z}+\frac{\partial w}{\partial x}\right)+e_{15}\frac{\partial \phi}{\partial x}+q_{15}\frac{\partial \psi}{\partial x}\right]\left(\frac{\partial \delta u}{\partial z}+\frac{\partial \delta w}{\partial x}\right)$$
$$+\left[C_{16}\frac{\partial u}{\partial x}+C_{36}\frac{\partial w}{\partial z}+C_{66}\frac{\partial v}{\partial x}+e_{16}\frac{\partial \phi}{\partial x}+e_{36}\frac{\partial \phi}{\partial z}+q_{16}\frac{\partial \psi}{\partial x}+q_{36}\frac{\partial \psi}{\partial z}\right]\frac{\partial \delta v}{\partial x}$$
$$-\rho\left(\frac{\partial^2 u}{\partial t^2}\delta u+\frac{\partial^2 v}{\partial t^2}\delta v+\frac{\partial^2 z}{\partial t^2}\delta w\right)\Bigg\}\,\mathrm{d}V-\oint_S(t_x\delta u+t_y\delta v+t_z\delta z)\,\mathrm{d}S, \tag{16}$$

$$0=\int_V\Bigg\{\left[e_{11}\frac{\partial u}{\partial x}+e_{14}\frac{\partial v}{\partial z}+e_{15}\left(\frac{\partial u}{\partial z}+\frac{\partial w}{\partial x}\right)+e_{16}\frac{\partial v}{\partial x}-\varepsilon_{11}\frac{\partial \phi}{\partial x}-d_{11}\frac{\partial \psi}{\partial x}\right]\frac{\partial \delta \phi}{\partial x}$$
$$+\left[e_{21}\frac{\partial u}{\partial x}+e_{24}\frac{\partial v}{\partial z}+e_{25}\left(\frac{\partial u}{\partial z}+\frac{\partial w}{\partial x}\right)+e_{26}\frac{\partial v}{\partial x}-\varepsilon_{12}\frac{\partial \phi}{\partial x}-d_{12}\frac{\partial \psi}{\partial x}\right]\frac{\partial \delta \phi}{\partial y}$$
$$+\left[e_{31}\frac{\partial u}{\partial x}+e_{33}\frac{\partial w}{\partial z}+e_{36}\frac{\partial v}{\partial x}-\varepsilon_{33}\frac{\partial \phi}{\partial z}-d_{33}\frac{\partial \psi}{\partial z}\right]\frac{\partial \delta \phi}{\partial z}\Bigg\}\,\mathrm{d}V-\oint_S D_j n_j\delta\phi\,\mathrm{d}S, \tag{17}$$

$$0=\int_V\Bigg\{\left[q_{11}\frac{\partial u}{\partial x}+q_{14}\frac{\partial v}{\partial z}+q_{15}\left(\frac{\partial u}{\partial z}+\frac{\partial w}{\partial x}\right)+q_{16}\frac{\partial v}{\partial x}-d_{11}\frac{\partial \phi}{\partial x}-\mu_{11}\frac{\partial \psi}{\partial x}\right]\frac{\partial \delta \psi}{\partial x}$$
$$+\left[q_{21}\frac{\partial u}{\partial x}+q_{24}\frac{\partial v}{\partial z}+q_{25}\left(\frac{\partial u}{\partial z}+\frac{\partial w}{\partial x}\right)+q_{26}\frac{\partial v}{\partial x}-d_{12}\frac{\partial \phi}{\partial x}-\mu_{12}\frac{\partial \psi}{\partial x}\right]\frac{\partial \delta \psi}{\partial y}$$
$$+\left[q_{31}\frac{\partial u}{\partial x}+q_{33}\frac{\partial w}{\partial z}+q_{36}\frac{\partial v}{\partial x}-d_{33}\frac{\partial \phi}{\partial z}-\mu_{33}\frac{\partial \psi}{\partial z}\right]\frac{\partial \delta \psi}{\partial z}\Bigg\}\,\mathrm{d}V-\oint_S B_j n_j\delta\psi\,\mathrm{d}S, \tag{18}$$

where u, v, and w represent the displacement components in the x-, y-, and z-directions, respectively, and ϕ and ψ represent the electric and magnetic potentials. It is important to mention here that Eq. (16) will actually result in three different equations when the coefficients of the variations of the mechanical displacements are collected.

2.4. Discrete-layer approximation and solution

The basic idea behind the Ritz method is to approximate the displacements u_i, and the electric and magnetic potentials ϕ and ψ by a finite linear combination of the form (see Refs. [23,24])

$$u_i(x,y,z,t)=\sum_{j=1}^{n}c_j^i\Gamma_j^{u_i}(x,y,z,t)+\Gamma_0^{u_i},$$

$$\phi(x,y,z,t)=\sum_{j=1}^{n}c_j\Gamma_j^{\phi}(x,y,z,t)+\Gamma_0^{\phi},$$

$$\psi(x,y,z,t)=\sum_{j=1}^{n}c_j\Gamma_j^{\psi}(x,y,z,t)+\Gamma_0^{\psi} \tag{19}$$

and then determine the parameters c_j to satisfy the principle of virtual displacements. Here, c_j denotes the undetermined coefficients, and Γ_j the approximation functions which must satisfy the boundary conditions and be continuous, as required by the variational principle.

Approximations to the three displacements (for elastic media), the three displacements and electrostatic potential (for piezoelectric media), and the three displacement and magnetic potential (for magnetostrictive media) are generated in terms of the global (x,y,z)-coordinates. In this study, the approximations for each of the five field quantities are constructed in such a way as to separate the dependence in the plane with that in the direction perpendicular to the interface. Additionally, the laminates are considered infinitely long in the

y-direction, eliminating the dependence of the approximations on the y-coordinate. Hence approximations for the five unknown field quantities are sought in the form

$$u(x,z,t)=\sum_{j=1}^{n}U_j(x,t)\Gamma_j^u(z)=\sum_{i=1}^{m}\sum_{j=1}^{n}U_{ji}(t)\Gamma_i^u(x)\Gamma_j^u(z),$$

$$v(x,z,t)=\sum_{j=1}^{n}V_j(x,t)\Gamma_j^v(z)=\sum_{i=1}^{m}\sum_{j=1}^{n}V_{ji}(t)\Gamma_i^v(x)\Gamma_j^v(z),$$

$$w(x,z,t)=\sum_{j=1}^{n}W_j(x,t)\Gamma_j^w(z)=\sum_{i=1}^{m}\sum_{j=1}^{n}W_{ji}(t)\Gamma_i^w(x)\Gamma_j^w(z),$$

$$\phi(x,z,t)=\sum_{j=1}^{n}\Phi_j(x,t)\Gamma_j^\phi(z)=\sum_{i=1}^{m}\sum_{j=1}^{n}\Phi_{ji}(t)\Gamma_i^\phi(x)\Gamma_j^\phi(z),$$

$$\psi(x,z,t)=\sum_{j=1}^{n}\Psi_j(x,t)\Gamma_j^\psi(z)=\sum_{i=1}^{m}\sum_{j=1}^{n}\Psi_{ji}(t)\Gamma_i^\psi(x)\Gamma_j^\psi(z). \tag{20}$$

In the thickness direction, one-dimensional Lagrangian interpolation polynomials are used for $\Gamma_j(z)$ for each of the five variables. For the in-plane approximations (i.e., that in the x-direction), different types of approximations can be used for the one-dimensional functions $\Gamma_j(x)$. Power and Fourier series are those most commonly selected. For a laminate with N layers through the parallelepiped thickness (typically taken equal to or greater than the number of different material laminae in the parallelepiped), $(N+1)$ is the number of layer interfaces through the parallelepiped thickness, and U_{ji}, V_{ji}, W_{ji}, Φ_{ji}, and Ψ_{ji} are constants associated with jth layer of the discretized laminate corresponding to the ith term of the in-plane approximation function for each of the five variables [25].

Substituting these approximations, Eq. (20), into the weak form in Eqs. (16)–(18), integrating with respect to the thickness coordinate z, collecting the coefficients of the variations of the displacements, and placing the results in matrix form yields the result

$$\begin{bmatrix}[M^{uu}] & [0] & [0] & [0] & [0]\\ [0] & [M^{vv}] & [0] & [0] & [0]\\ [0] & [0] & [M^{ww}] & [0] & [0]\\ [0] & [0] & [0] & [0] & [0]\\ [0] & [0] & [0] & [0] & [0]\end{bmatrix}\begin{Bmatrix}\{\ddot{u}\}\\ \{\ddot{v}\}\\ \{\ddot{w}\}\\ \{0\}\\ \{0\}\end{Bmatrix}$$
$$+\begin{bmatrix}[K^{uu}] & [K^{uv}] & [K^{uw}] & [K^{u\phi}] & [K^{u\psi}]\\ [K^{vu}] & [K^{vv}] & [K^{vw}] & [K^{v\phi}] & [K^{v\psi}]\\ [K^{wu}] & [K^{wv}] & [K^{ww}] & [K^{w\phi}] & [K^{w\psi}]\\ [K^{\phi u}] & [K^{\phi v}] & [K^{\phi w}] & [K^{\phi\phi}] & [K^{\phi\psi}]\\ [K^{\psi u}] & [K^{\psi v}] & [K^{\psi w}] & [K^{\psi\phi}] & [K^{\psi\psi}]\end{bmatrix}\begin{Bmatrix}\{u\}\\ \{v\}\\ \{w\}\\ \{\phi\}\\ \{\psi\}\end{Bmatrix}=\begin{Bmatrix}\{f^u\}\\ \{f^v\}\\ \{f^w\}\\ \{f^\phi\}\\ \{f^\psi\}\end{Bmatrix}. \tag{21}$$

The elements of each of these matrices have a very specific form as a result of the pre-integration of the thickness dependence. The matrices are in fact composed of smaller sub-matrices that consist of the fully integrated thickness approximation functions multiplied by the various in-plane functions. The explicit form of each of these sub-matrices contained in the stiffness matrix $[K]$ and the inertial mass matrix $[M]$ are given in Appendix B before integrating with respect to thickness coordinate and before the insertion of the specific discrete-layer approximations.

The dynamic analysis of the laminates is developed assuming harmonic motion. Therefore, the solutions for the primary unknowns have the form

$$u_i(x,z,t) = u_i(x,z)\mathrm{e}^{\mathrm{i}\omega t}, \tag{22}$$

$$\phi(x,z,t) = \phi(x,z)\mathrm{e}^{\mathrm{i}\omega t}, \tag{23}$$

$$\psi(x,z,t) = \psi(x,z)\mathrm{e}^{\mathrm{i}\omega t}, \tag{24}$$

where ω is the natural frequency.

Taking second derivative with respect to time of Eqs. (22)–(24) gives

$$\ddot{u}_i(x,z,t) = -\omega^2 u_i(x,z)\mathrm{e}^{\mathrm{i}\omega t}, \tag{25}$$

$$\ddot{\phi}(x,z,t) = -\omega^2 \phi(x,z)\mathrm{e}^{\mathrm{i}\omega t}, \tag{26}$$

$$\ddot{\psi}(x,z,t) = -\omega^2 \psi(x,z)\mathrm{e}^{\mathrm{i}\omega t}. \tag{27}$$

Replacing Eqs. (25)–(27) into Eq. (21), and simplifying the dynamic problem becomes the following *e*-value problem:

$$\begin{bmatrix} [K^{uu}] & [K^{uv}] & [K^{uw}] & [K^{u\phi}] & [K^{u\psi}] \\ [K^{vu}] & [K^{vv}] & [K^{vw}] & [K^{v\phi}] & [K^{v\psi}] \\ [K^{wu}] & [K^{wv}] & [K^{ww}] & [K^{w\phi}] & [K^{w\psi}] \\ [K^{\phi u}] & [K^{\phi v}] & [K^{\phi w}] & [K^{\phi\phi}] & [K^{\phi\psi}] \\ [K^{\psi u}] & [K^{\psi v}] & [K^{\psi w}] & [K^{\psi\phi}] & [K^{\psi\psi}] \end{bmatrix} \begin{Bmatrix} \{u\} \\ \{v\} \\ \{w\} \\ \{\phi\} \\ \{\psi\} \end{Bmatrix}$$
$$- \omega^2 \begin{bmatrix} [M^{uu}] & [0] & [0] & [0] & [0] \\ [0] & [M^{vv}] & [0] & [0] & [0] \\ [0] & [0] & [M^{ww}] & [0] & [0] \\ [0] & [0] & [0] & [0] & [0] \\ [0] & [0] & [0] & [0] & [0] \end{bmatrix} \begin{Bmatrix} \{u\} \\ \{v\} \\ \{w\} \\ \{0\} \\ \{0\} \end{Bmatrix} = \begin{Bmatrix} \{0\} \\ \{0\} \\ \{0\} \\ \{0\} \\ \{0\} \end{Bmatrix}. \tag{28}$$

The natural frequencies and the corresponding shape functions can be found by solving this eigenvalue problem with no external forces since free vibration analysis is assumed. The electric and magnetic potentials are eliminated from this equation by following a standard matrix condensation procedure, allowing solution by using direct eigensolvers. First, we consider the following partition of the matrix equation (28):

$$\begin{bmatrix} [K^{UU}] & [K^{U\Phi}] \\ [K^{\Phi U}] & [K^{\Phi\Phi}] \end{bmatrix} \begin{Bmatrix} \{U\} \\ \{\Phi\} \end{Bmatrix} - \omega^2 \begin{bmatrix} [M^{UU}] & [0] \\ [0] & [0] \end{bmatrix} \begin{Bmatrix} \{U\} \\ \{0\} \end{Bmatrix} = \begin{Bmatrix} \{0\} \\ \{0\} \end{Bmatrix} \tag{29}$$

expanding Eq. (29) gives the matrix equations

$$[K^{UU}]\{U\} + [K^{U\Phi}]\{\Phi\} - \omega^2[M^{UU}]\{U\} = \{0\}, \tag{30}$$

$$[K^{\Phi U}]\{U\} + [K^{\Phi\Phi}]\{\Phi\} = \{0\}. \tag{31}$$

Solving for Φ from Eq. (31) and substituting back in Eq. (29) results in the following general eigenvalue problem:

$$([\bar{K}] - \omega^2[M])\{U\} = \{0\}, \tag{32}$$

where U represents the modes shapes, ω is the natural frequency, and the condensed stiffness matrix $[\bar{K}]$ is calculated as

$$[\bar{K}] = ([K^{UU}] - [K^{U\Phi}][K^{\Phi\Phi}]^{-1}[K^{\Phi U}]). \tag{33}$$

3. Numerical examples

Three examples are considered in this section to study the free vibration behavior of linear magneto-electro-elastic laminates. First, a single-layer linear elastic piezoelectric plate, with known exact solution [8] is examined in order to validate the approximate model presented here. Then, a two-layer cantilever composite plate with the bottom layer made of the linear elastic graphite-epoxy, and the top layer made of the linear elastic piezoelectric PZT-5A is studied and results are compared to those presented by Vel et al. [21]. Finally, a two-layer cantilever magneto-electro-elastic plate with the bottom layer made of the linear magnetostrictive material $CoFe_2O_4$ and the top layer of the linear piezoelectric $BaTiO_3$ is analyzed.

3.1. Single-layer simply supported piezoelectric plate

The first example considered is a single-layer homogeneous plate made of the piezoelectric PZT-4 with material properties shown in Table 1. A plate with dimensions $L_x = 0.04$ m and total thickness $H = 0.01$ m is modelled. The edge boundary conditions are consistent with those of simple support. Hence, the transverse displacement w is specified to be zero, with zero normal traction also specified along the edge length and along the top and bottom surfaces of the laminate. In terms of the electric and magnetic field variables, they are zero along the edges, as well as along the top and bottom surfaces of the laminate.

The in-plane approximation functions for each of the five field variables are given in the form

$$\Gamma_j^u(x) = \cos px, \tag{34}$$

$$\Gamma_j^v(x) = \cos px, \tag{35}$$

$$\Gamma_j^w(x) = \sin px, \tag{36}$$

$$\Gamma_j^\phi(x) = \sin px, \tag{37}$$

$$\Gamma_j^\Psi(x) = \sin px, \tag{38}$$

where $p = n\pi/L_x$. Here, the index j is a single integer that represents the axial mode number denoted by p in each of the terms. In this example, only one term is required to match the exact solution corresponding to the first axial mode (i.e., $n = 1$) as published by Heyliger and Brooks [8].

The natural frequencies are normalized as

$$\overline{\omega}_n = \omega_n(L_x^2/H)\sqrt{(\rho/C_{11})}, \tag{39}$$

where L_x is the span length of the plate, H is the thickness, ρ and C_{11} are the mass density and the corresponding element of the elastic stiffness matrix (see Table 1), and ω_n is the nth frequency found in the analysis.

The first 5 natural frequencies obtained using the present approach are shown in Table 2 and are in excellent agreement with the exact frequencies reported by Heyliger and Brooks [8], and with finite elements results obtained using ABAQUS 6.1 [26]. A convergence analysis using different number of layers for the discrete layer approximation was also performed and is shown in Table 3. The corresponding mode shapes are shown in Fig. 2 for the first four vibration modes.

It can be determined from Table 3 that when 16 layers are used in the discrete layer solution, the calculated frequencies can be within an error of only 0.5%, and within 0.2% when the laminate is discretized into 128 layers. Using 16 layers results in a system of equations with 68 degrees of freedom, and using 128 layers the

Table 2
Normalized natural frequencies for the simply supported PZT-4 one-layer plate

Mode	Present solution discrete layer	Heyliger and Brooks exact solution	ABAQUS finite elements
1	2.265	2.261	2.265
2	10.087	10.082	10.087
3	24.089	24.086	24.089
4	41.675	41.700	41.679
5	49.524	49.616	49.522

Table 3
Convergence analysis for the simply supported PZT-4 one-layer plate

Frequency	4 Layers	8 Layers	16 Layers	32 Layers	64 Layers	128 Layers
1	2.286	2.271	2.266	2.265	2.265	2.265
2	10.090	10.088	10.087	10.087	10.087	10.087
3	24.721	24.246	24.128	24.099	24.091	24.089
4	44.910	42.549	41.893	41.727	41.685	41.675
5	51.952	50.072	49.656	49.555	49.531	49.524

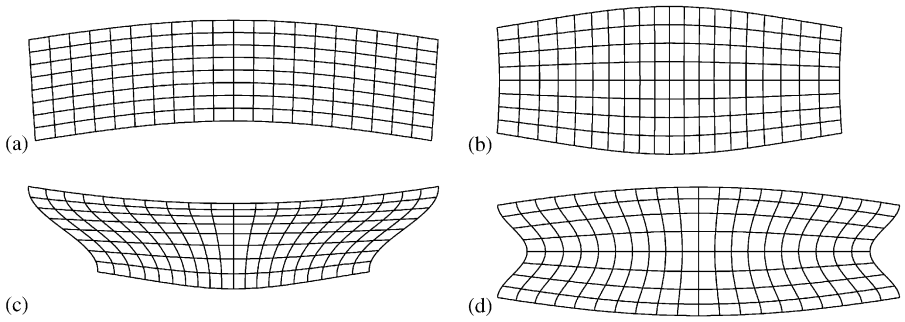

Fig. 2. First 4 mode shapes for the simply supported PZT-4 one-layer plate (side views): (a) Mode 1, (b) Mode 2, (c) Mode 3, and (d) Mode 4.

number of degrees of freedom is 516. Although not shown here, a convergence analysis using finite elements was also performed and showed that 1024 (4420 dof) elements are required to obtain an error within 0.5% when using 4-node elements, or 64 elements (932 dof) when 8-node elements are used. In order to obtain an error smaller than 0.2% 4096 (17 028 dof) 4-node elements are required, or 256 (3396 dof) 8-node elements. It is clear then, that a significant reduction in the computational requirements is achieved when the present discrete model is employed, without losing accuracy in the calculated frequencies.

3.2. Two-layer PZT-5A/graphite-epoxy cantilever plate

This example is considered here in order to give a second validation to the present model by comparing the natural frequencies to those published by Vel et al. [21] using an analytical solution.

The problem considered in this example is a cantilever two-layer laminated plate with the top layer made of the piezoelectric material PZT-5A, and the bottom layer made of graphite-epoxy with the fibers oriented in the direction of the span of the laminate. The plate has dimensions $L_x = 0.1$ m, total thickness $H = 0.025$ m, and the two dissimilar layers have equal thickness. The support of the plate is at the left edge with mechanical displacements specified to zero. The right edge, top, and bottom surfaces are traction free. The edges and top

surface of the PZT-5A are grounded to zero electric and magnetic potential, as well as the interface between the two different materials. The corresponding material properties can be found in Table 1.

For this example, the approximation functions are different to those used in the previous example. In this case, in order to satisfy the boundary conditions, the in-plane functions for u, w, ϕ, and ψ are selected as power series in x given as

$$\Gamma_j^u(x) = x^n, \tag{40}$$

$$\Gamma_j^v(x) = x^n, \tag{41}$$

$$\Gamma_j^w(x) = x^n, \tag{42}$$

$$\Gamma_j^\phi(x) = x^n(x - L_x), \tag{43}$$

$$\Gamma_j^\Psi(x) = x^n(x - L_x). \tag{44}$$

The natural frequencies were calculated using the discrete layer approach, the commercial finite elements software ABAQUS, and a finite element program developed by the authors. The first 10 normalized natural frequencies obtained using the mentioned methods and those presented by Vel et al. [21] are listed in Table 4. The natural frequencies are normalized using Eq. (39) with $\rho = 7750\,\mathrm{kg/m^3}$, and $C_{11} = 99.201\,\mathrm{GPa}$. Excellent agreement is obtained for the natural frequencies among the discrete layer, ABAQUS, and FE results. However, they are different from the analytical values presented by Vel et al. [21]. The first six modal shapes are illustrated in Fig. 3, and they coincide to those published by Vel et al. [21].

Since the analytical results were validated by Vel et al. [21] using ABAQUS, and because good agreement is found between modal shapes, it is possible that the discrepancies in the natural frequencies are due to differences between material properties used in this work and the values used by Vel et al. [21].

Convergence analyses were also completed for this example using 4, 8, 16, 32, and 64 layers in the discretization of the plate thickness, and 4, 6, 8, 10, and 12 terms in the approximation functions. The convergence analysis is shown in Table 5 for the first natural frequency, and the maximum error relative to converged values for the first five frequencies as a function of number of layers and terms is presented in Table 6. For the first frequency, when 16 layers and 6 terms are employed with 408 degrees of freedom, an error of 0.40% is obtained. Finite element analyses using 256 4-node elements (1188 dof) or 64 8-node elements (932 dof) result in the same error for the first natural frequency. When 16 layers and 8 terms (544 dof) are used in our discrete layer approach, a maximum error of 0.23% is obtained in the calculation of the first 5 frequencies. The same accuracy is obtained with finite element analyses when 1024 (4420 dof) 4-node elements are used, or when 64 (932 dof) 8-node elements are employed. This is consistent with the general behavior of the Ritz method versus finite element models.

Table 4
Normalized natural frequencies for the two-layer PZT-5A/graphite-epoxy cantilever plate

Frequency	Discrete layer	ABAQUS	Finite elements	Vel et al. [21]
1	1.190	1.189	1.190	1.114
2	4.840	4.837	4.841	4.316
3	8.590	8.587	8.590	8.015
4	10.623	10.618	10.625	9.737
5	16.369	16.360	16.373	15.160
6	19.857	19.852	19.856	18.930
7	22.888	22.874	22.894	21.390
8	28.235	28.219	28.235	26.670
9	29.767	29.746	29.765	28.530
10	32.842	32.814	32.826	29.380

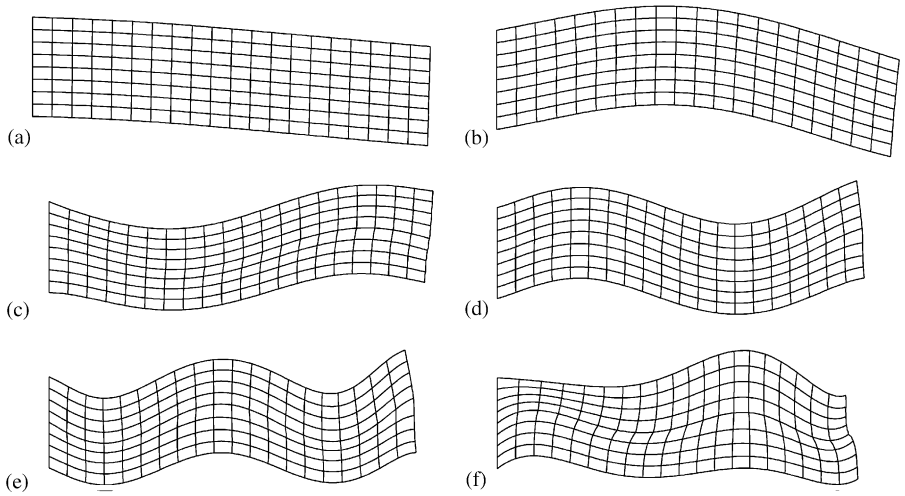

Fig. 3. First 6 mode shapes for the two-layer PZT-5A/graphite-epoxy cantilever plate (side views): (a) Mode 1, (b) Mode 2, (c) Mode 3, (d) Mode 4, (e) Mode 5, and (f) Mode 6.

Table 5
Convergence analysis for the first natural frequency of the two-layer PZT-5A/graphite-epoxy cantilever plate

Layers	Terms				
	4	6	8	10	12
4	1.2117	1.2045	1.2023	1.2016	1.2014
8	1.2047	1.1973	1.1945	1.1936	1.1932
16	1.2028	1.1949	1.1922	1.1912	1.1907
32	1.2023	1.1944	1.1916	1.1906	1.1903
64	1.2022	1.1915	1.1908	1.1904	1.1899

Table 6
Maximum error in the calculation of the first 5 natural frequencies for the two-layer PZT-5A/graphite-epoxy cantilever plate

Layers	Terms				
	4	6	8	10	12
4	23.7482	4.0053	1.8572	1.7966	1.7887
8	22.3941	2.8357	0.6844	0.6138	0.6025
16	21.9979	2.3819	0.2347	0.1556	0.1383
32	21.8932	2.2493	0.1326	0.0412	0.0031
64	21.8663	2.2463	0.1198	0.0272	0.0030

3.3. *Two-layer $BaTiO_3/CoFe_2O_4$ cantilever plate*

As a final example, a direct application of the presented discrete layer approach to the free vibration of a magneto-electro-elastic laminated plate is studied. In this case a two-layer cantilever plate with the top layer made of the piezoelectric material $BaTiO_3$ and bottom layer made of the magnetostrictive material $CoFe_2O_4$ is considered (the material properties are again shown in Table 1). The span length is $L_x = 0.1\,\text{m}$, the total thickness is $H = 0.025\,\text{m}$, and both layers have again the same thickness. The boundary conditions are: along

the left edge of the laminate the mechanical displacements u, v, and w are set to zero, and the right edge, top, and bottom surfaces are traction free. Both edges of the plate, as well as the top and bottom surfaces, are grounded to zero electric and magnetic potential. The approximation functions for this example are the same as those used in the previous example and they are shown in Eqs. (40)–(44).

The natural frequencies are normalized according to Eq. (39) with $\rho = 5800\,\mathrm{kg/m^3}$, and $C_{11} = 286.0\,\mathrm{GPa}$. The first 10 natural frequencies calculated using the discrete layer approach are listed in Table 7 along with results using the finite element method, excellent agreement is obtained. The first 6 modal shapes are presented in Fig. 4, with a significant change in the laminate thickness observed for modes 3 and 5.

In Table 8, the convergence analysis for the first frequency is shown. Using 16 layers, 8 terms, and 544 degrees of freedom in our approximation resulted in an error of 0.38% for the first natural frequency. In order to obtain a smaller error using finite elements, 1024 (4420 dof) 4-node elements or 64 (932 dof) 8-node elements are required. The maximum error found in the calculation of first 5 frequencies for different number of layers and terms in our discrete layer approximation are listed in Table 9. Once again the computational advantages of the present approach are clear. The discrete layer approach results in 1584 degrees of freedom with a maximum error of 0.09%, while the finite element approach requires 4420 or 3396 degrees of freedom when 4-node or 8-node elements are used.

Table 7
Normalized natural frequencies for the two-layer $BaTiO_3/CoFe_2O_4$ cantilever plate

Frequency	Discrete layer	Finite elements
1	0.729	0.729
2	3.581	3.581
3	4.817	4.816
4	8.161	8.157
5	12.959	12.956
6	14.155	14.152
7	17.952	17.946
8	21.213	21.212
9	22.451	22.447
10	24.011	24.003

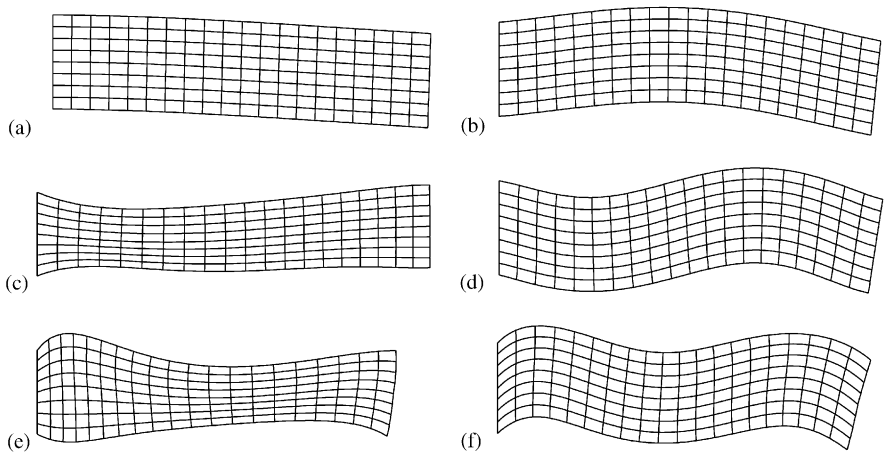

Fig. 4. First 6 mode shapes for the two-layer $BaTiO_3/CoFe_2O_4$ cantilever plate (side views): (a) Mode 1, (b) Mode 2, (c) Mode 3, (d) Mode 4, (e) Mode 5, and (f) Mode 6.

Table 8
Convergence analysis for the first natural frequency of the two-layer $BaTiO_3/CoFe_2O_4$ cantilever plate

Layers	Terms				
	4	6	8	10	12
4	0.7511	0.7432	0.7408	0.7401	0.7398
8	0.7441	0.7357	0.7331	0.7321	0.7316
16	0.7423	0.7337	0.7309	0.7295	0.7294
32	0.7419	0.7333	0.7304	0.7293	0.7288
64	0.7417	0.7331	0.7302	0.7291	0.7286

Table 9
Maximum error in the calculation of the first 5 natural frequencies for the two-layer $BaTiO_3/CoFe_2O_4$ cantilever plate

Layers	Terms				
	4	6	8	10	12
4	16.6287	3.8082	1.8683	1.8251	1.8198
8	15.9857	2.5843	0.6691	0.5649	0.5534
16	15.8178	2.2053	0.3842	0.1906	0.1736
32	15.7755	2.1042	0.313	0.1589	0.0901
64	15.7649	2.0785	0.2951	0.1395	0.0703

The through-thickness variations of the in-plane displacement u, out-of-plane displacement w, electric potential ϕ, and magnetic potential ψ at $x = L/4$ and $3L/4$ are shown in Fig. 5 for the first 4 natural modes. The electric potential displays a nonlinear variation in the piezoelectric media, while its variation is linear in the magnetostrictive media. The opposite behavior is observed for the magnetic potential, that is, nonlinear in the magnetostrictive media, and linear in the piezoelectric media. The through-thickness behavior of the vertical displacement w is effectively constant for modes 1, 2, and 4, indicating that those modes are primary bending modes. For mode 3, the through-thickness variation of the in-plane displacement is constant, indicating that this mode is a predominant axial vibration mode.

The influence of the piezoelectric and piezomagnetic coefficients on the natural frequencies of the cantilever plate was also studied. Each of these coefficients was allowed to vary from zero to four times its actual value, and the natural frequencies were calculated while keeping the other coefficients unchanged. Results of this analysis are shown in Figs. 6 and 7. In these figures, ω/ω_0 represents the ratio of the calculated frequency to the frequency obtained using the actual coefficients for the corresponding vibration mode, e/e_0 represents the ratio of the used value of the corresponding piezoelectric coefficient to its actual value, and q/q_0 represents the ratio of the used value of the corresponding piezomagnetic coefficient to its actual value. Not surprisingly, the magnitude of the natural frequencies increases as the piezoelectric and piezomagnetic coefficients become higher, indicating a stiffening effect caused by the coupling among elastic, electric and magnetic fields. The piezoelectric and piezomagnetic coefficients have a similar level of influence on the natural frequencies of the plate, with e_{31} and q_{31} having the highest impact for the first three vibration modes. The natural frequency corresponding to the fourth vibration mode is more affected by the e_{15} and q_{15} coefficients which represent the coupling between electric and magnetic fields with the shear strain. In this mode shape, as well as in mode 2, there is an important contribution of shear deformation to the vibration behavior of the plate. This can be observed in the modal shapes shown in Fig. 4. It is not surprising to see the presence of a shearing vibration mode since the laminate is considered a thick

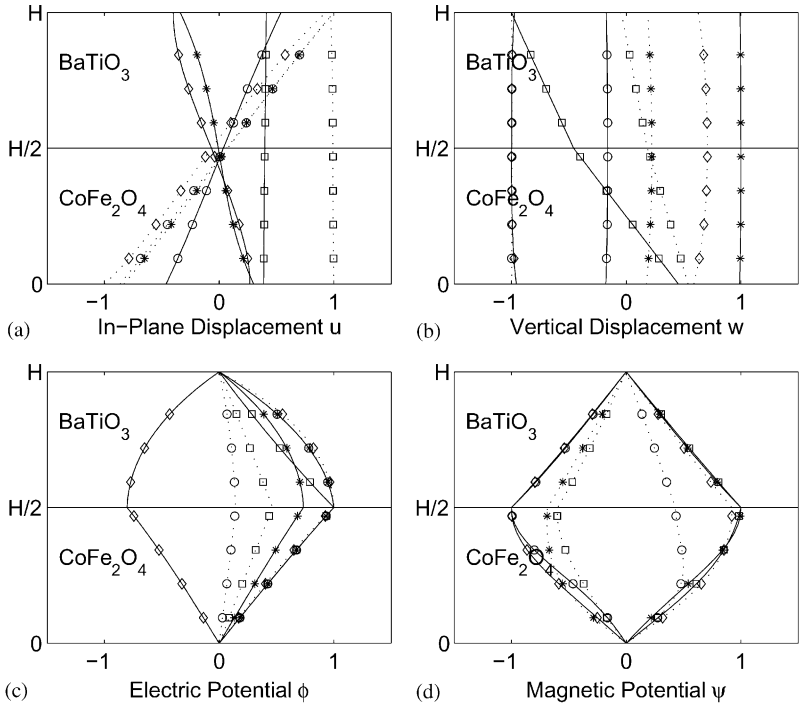

Fig. 5. Through-thickness variation of main fields for the first 4 vibration modes of the two-layer $BaTiO_3/CoFe_2O_4$ cantilever plate: (a) in-plane displacement u, (b) vertical displacement w, (c) electric potential ϕ, and (d) magnetic potential ψ. The variation of the fields at $x = L_x/4$ is represented by solid lines, and dotted lines represent their variation at $x = 3L_x/4$. Open circles, stars, open squares, and open diamonds indicate modes 1, 2, 3, and 4, respectively.

plate with aspect ratio $L_x/H = 4$, and this behavior is expected to change when thin laminates with higher aspect ratio are studied.

4. Conclusions

A discrete layer model has been presented for the solution of the free vibration of two-dimensional linear magneto-electro-elastic laminated plates. Approximations for the three mechanical displacements, electric potential, and magnetic potential are expressed as functions of the global coordinates with separate dependence on the in-plane coordinate x, and the out-of-plane coordinate z. The present model was validated with excellent agreement by comparing the natural frequencies of a simply supported homogeneous PZT-4 plate with the exact solution results [8]. We also validated this model by comparing the frequencies of a two-layer PZT-5A/graphite-epoxy plate with a recent analytical solution [21], with results obtained using the commercial finite element software ABAQUS, and with results obtained from a finite element program developed by the authors. Finally, the present approach was used to study the free vibration behavior of a two-layer magneto-electro-elastic plate made of the piezoelectric material $BaTiO_3$ and the magnetostrictive material $CoFe_2O_4$.

For the specimen geometries and material properties used in the present work, we conclude the following:

1. The discrete-layer model can be used to solve the free-vibration problem of magneto-electro-elastic laminated plates with excellent accuracy when a sufficient number of layers and terms are employed in the approximations. Using 128 layers and one approximation term for the simply supported PZT-4, and 32 layers and 12 terms for cantilever plates resulted in 3–4 digits of accuracy.

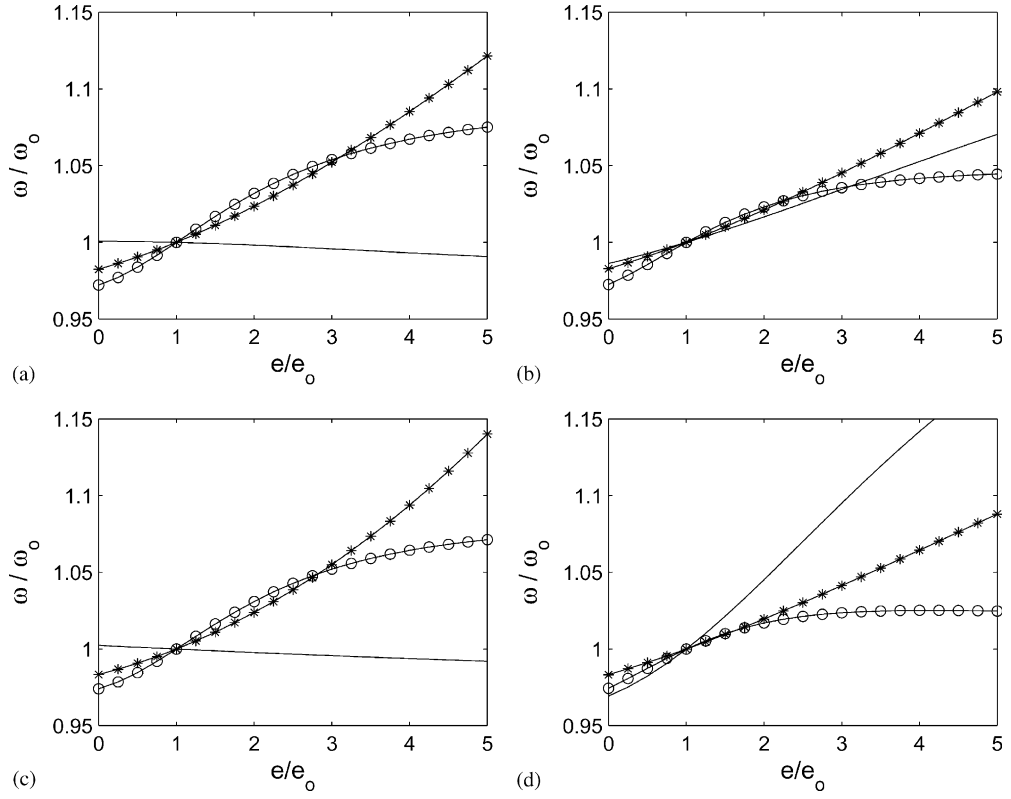

Fig. 6. Influence of piezoelectric coefficients on the natural frequencies of the two-layer $BaTiO_3/CoFe_2O_4$ cantilever plate: (a) Mode 1, (b) Mode 2, (c) Mode 3, and (d) Mode 4. Solid lines, stars, and open circles represent e_{15}, e_{31}, and e_{33}, respectively.

2. Satisfactory levels of accuracy can be obtained using the present approach using a fairly small number of layers and terms for the approximation functions. Less than 1.0% error was achieved with 68 layers and 1 approximation term for the simply supported plate, and 8 layers and 8 approximation terms for the cantilever laminates.
3. For the same level of accuracy, the present approach results in a smaller number of degrees of freedom when compared to finite element analyses, with the consequent reduction in computational time. For the simply supported laminate the number of degrees of freedom using the discrete layer approach was about 14 times smaller than that required by the finite element method to obtain a maximum error smaller than 0.5%, and about 2 times smaller for the case of cantilever plates.
4. It was observed during the analysis of the magneto-electro-elastic cantilever plate, that the through-thickness behavior of the electric potential is nonlinear within the piezoelectric layer, while it is linear within the magnetostrictive layer. The opposite behavior was observed for the magnetic potential. Subsequent simplified models could exploit this behavior.
5. Consistent with earlier observations, higher piezoelectric or piezomagnetic coefficients resulted in higher natural frequencies. Therefore, there is a general stiffening effect due to the coupled elastic, electric, and magnetic fields.
6. The piezoelectric coefficients and piezomagnetic coefficients exhibit a similar level of influence on the natural frequencies of the magneto-electro-elastic plate studied here. Maximum increments in the corresponding frequency were between 10.0% and 13.0% for mode 1, 4.0% to 10.0% for mode 2, about 14.0% for mode 3, and between 12.0% and 20.0% for mode 4. It was also observed that for the first three vibration modes the piezoelectric coefficient with highest impact on the frequencies is e_{31}, while q_{31} has the highest impact among the different piezomagnetic coefficients. However, for mode 4 the e_{15} and q_{15} coefficients showed a higher influence on the natural vibration frequencies of the laminate indicating a

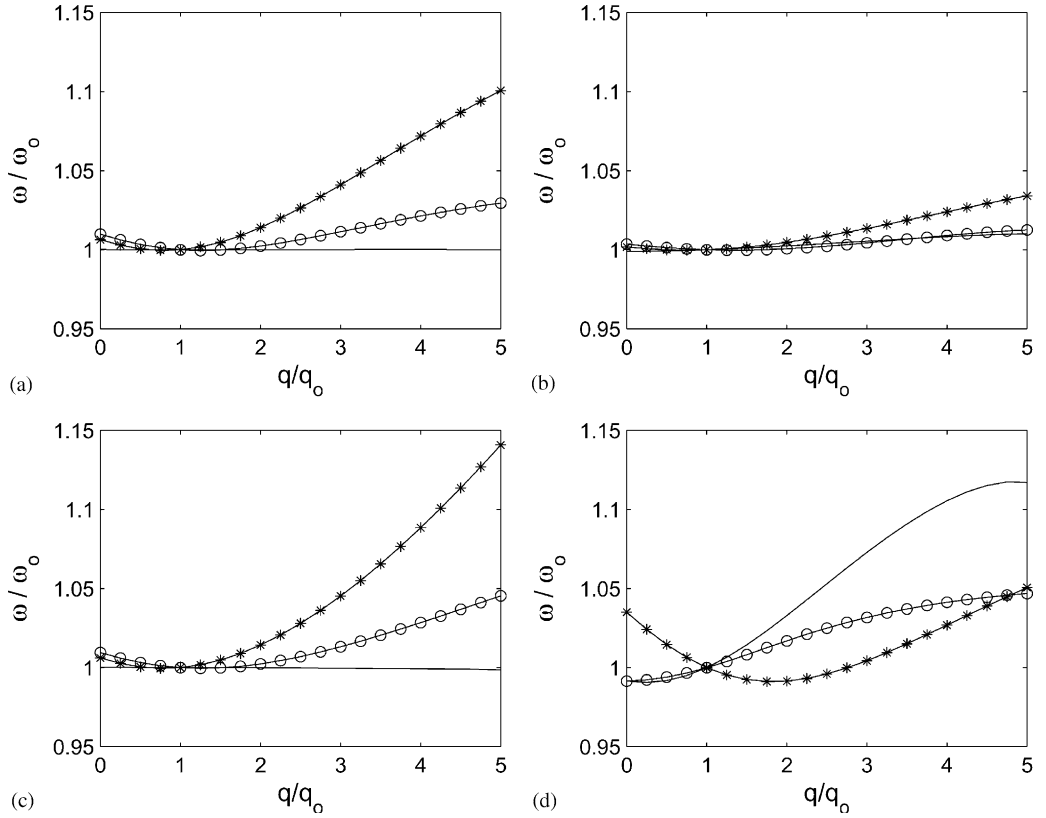

Fig. 7. Influence of piezomagnetic coefficients on the natural frequencies of the two-layer $BaTiO_3/CoFe_2O_4$ cantilever plate: (a) Mode 1, (b) Mode 2, (c) Mode 3, and (d) Mode 4. Solid lines, stars, and open circles represent q_{15}, q_{31}, and q_{33}, respectively.

primary shearing vibration mode. Modal shapes with a predominant shear deformation are expected to be present for thick plates as those considered here, and this behavior would change as the aspect ratio of the plate is increased.

Appendix A

Elastic stiffness tensor:

$$[C] = \begin{bmatrix} C_{11} & C_{12} & C_{13} & 0 & 0 & 0 \\ C_{12} & C_{22} & C_{23} & 0 & 0 & 0 \\ C_{13} & C_{23} & C_{33} & 0 & 0 & 0 \\ 0 & 0 & 0 & C_{44} & 0 & 0 \\ 0 & 0 & 0 & 0 & C_{55} & 0 \\ 0 & 0 & 0 & 0 & 0 & C_{66} \end{bmatrix}.$$

Dielectric permittivity constants:

$$[\varepsilon] = \begin{bmatrix} \varepsilon_{11} & 0 & 0 \\ 0 & \varepsilon_{22} & 0 \\ 0 & 0 & \varepsilon_{33} \end{bmatrix}.$$

Magnetic permittivity constants:

$$[\mu] = \begin{bmatrix} \mu_{11} & 0 & 0 \\ 0 & \mu_{22} & 0 \\ 0 & 0 & \mu_{33} \end{bmatrix}.$$

Piezoelectric coefficients:

$$[e] = \begin{bmatrix} 0 & 0 & 0 & 0 & e_{15} & 0 \\ 0 & 0 & 0 & e_{24} & 0 & 0 \\ e_{31} & e_{32} & e_{33} & 0 & 0 & 0 \end{bmatrix}.$$

Piezomagnetic coefficients:

$$[q] = \begin{bmatrix} 0 & 0 & 0 & 0 & q_{15} & 0 \\ 0 & 0 & 0 & q_{24} & 0 & 0 \\ q_{31} & q_{32} & q_{33} & 0 & 0 & 0 \end{bmatrix}.$$

Magnetoelectric coefficients:

$$[d] = \begin{bmatrix} d_{11} & 0 & 0 \\ 0 & d_{22} & 0 \\ 0 & 0 & d_{33} \end{bmatrix}.$$

Appendix B

$$M_{ij}^{uu} = \int_V [\rho \Gamma_i^u \Gamma_j^u] \, \mathrm{d}V, \tag{45}$$

$$M_{ij}^{vv} = \int_V [\rho \Gamma_i^v \Gamma_j^v] \, \mathrm{d}V, \tag{46}$$

$$M_{ij}^{ww} = \int_V [\rho \Gamma_i^w \Gamma_j^w] \, \mathrm{d}V, \tag{47}$$

$$K_{ij}^{uu} = \int_V \left[C_{11} \frac{\partial \Gamma_i^u}{\partial x} \frac{\partial \Gamma_j^u}{\partial x} + C_{55} \frac{\partial \Gamma_i^u}{\partial z} \frac{\partial \Gamma_j^u}{\partial z} \right] \mathrm{d}V, \tag{48}$$

$$K_{ij}^{uv} = \int_V \left[C_{14} \frac{\partial \Gamma_i^u}{\partial x} \frac{\partial \Gamma_j^v}{\partial z} + C_{45} \frac{\partial \Gamma_i^u}{\partial z} \frac{\partial \Gamma_j^v}{\partial z} + C_{16} \frac{\partial \Gamma_i^u}{\partial x} \frac{\partial \Gamma_j^v}{\partial x} \right] \mathrm{d}V, \tag{49}$$

$$K_{ij}^{uw} = \int_V \left[C_{13} \frac{\partial \Gamma_i^u}{\partial x} \frac{\partial \Gamma_j^w}{\partial z} + C_{55} \frac{\partial \Gamma_i^u}{\partial z} \frac{\partial \Gamma_j^w}{\partial x} \right] \mathrm{d}V, \tag{50}$$

$$K_{ij}^{u\phi} = \int_V \left[e_{11} \frac{\partial \Gamma_i^u}{\partial x} \frac{\partial \Gamma_j^\phi}{\partial x} + e_{31} \frac{\partial \Gamma_i^u}{\partial x} \frac{\partial \Gamma_j^\phi}{\partial z} + e_{15} \frac{\partial \Gamma_i^u}{\partial z} \frac{\partial \Gamma_j^\phi}{\partial x} \right] \mathrm{d}V, \tag{51}$$

$$K_{ij}^{u\psi} = \int_V \left[q_{11} \frac{\partial \Gamma_i^u}{\partial x} \frac{\partial \Gamma_j^\psi}{\partial x} + q_{31} \frac{\partial \Gamma_i^u}{\partial x} \frac{\partial \Gamma_j^\psi}{\partial z} + q_{15} \frac{\partial \Gamma_i^u}{\partial z} \frac{\partial \Gamma_j^\psi}{\partial x} \right] \mathrm{d}V, \tag{52}$$

$$K_{ij}^{vv} = \int_V \left[C_{44} \frac{\partial \Gamma_i^v}{\partial z} \frac{\partial \Gamma_j^v}{\partial z} + C_{66} \frac{\partial \Gamma_i^v}{\partial x} \frac{\partial \Gamma_j^v}{\partial x} \right] \mathrm{d}V, \tag{53}$$

$$K_{ij}^{vw} = \int_V \left[C_{45} \frac{\partial \Gamma_i^v}{\partial z} \frac{\partial \Gamma_j^w}{\partial x} + C_{36} \frac{\partial \Gamma_i^v}{\partial x} \frac{\partial \Gamma_j^w}{\partial z} \right] \mathrm{d}V, \tag{54}$$

$$K_{ij}^{v\phi} = \int_V \left[e_{14} \frac{\partial \Gamma_i^v}{\partial z} \frac{\partial \Gamma_j^\phi}{\partial x} + e_{16} \frac{\partial \Gamma_i^v}{\partial x} \frac{\partial \Gamma_j^\phi}{\partial x} + e_{36} \frac{\partial \Gamma_i^v}{\partial x} \frac{\partial \Gamma_j^\phi}{\partial z} \right] \mathrm{d}V, \tag{55}$$

$$K_{ij}^{v\psi} = \int_V \left[q_{14} \frac{\partial \Gamma_i^v}{\partial z} \frac{\partial \Gamma_j^\psi}{\partial x} + q_{16} \frac{\partial \Gamma_i^v}{\partial x} \frac{\partial \Gamma_j^\psi}{\partial x} + q_{36} \frac{\partial \Gamma_i^v}{\partial x} \frac{\partial \Gamma_j^\psi}{\partial z} \right] \mathrm{d}V, \tag{56}$$

$$K_{ij}^{ww} = \int_V \left[C_{33} \frac{\partial \Gamma_i^w}{\partial z} \frac{\partial \Gamma_j^w}{\partial z} + C_{55} \frac{\partial \Gamma_i^w}{\partial x} \frac{\partial \Gamma_j^w}{\partial x} \right] \mathrm{d}V, \tag{57}$$

$$K_{ij}^{w\phi} = \int_V \left[e_{33} \frac{\partial \Gamma_i^w}{\partial z} \frac{\partial \Gamma_j^\phi}{\partial z} + e_{15} \frac{\partial \Gamma_i^w}{\partial x} \frac{\partial \Gamma_j^\phi}{\partial x} \right] \mathrm{d}V, \tag{58}$$

$$K_{ij}^{w\psi} = \int_V \left[q_{33} \frac{\partial \Gamma_i^w}{\partial z} \frac{\partial \Gamma_j^\psi}{\partial z} + q_{15} \frac{\partial \Gamma_i^w}{\partial x} \frac{\partial \Gamma_j^\psi}{\partial x} \right] \mathrm{d}V, \tag{59}$$

$$K_{ij}^{\phi\phi} = \int_V \left[-\varepsilon_{11} \frac{\partial \Gamma_i^\phi}{\partial x} \frac{\partial \Gamma_j^\phi}{\partial x} - \varepsilon_{33} \frac{\partial \Gamma_i^\phi}{\partial z} \frac{\partial \Gamma_j^\phi}{\partial z} \right] \mathrm{d}V, \tag{60}$$

$$K_{ij}^{\phi\psi} = \int_V \left[-d_{11} \frac{\partial \Gamma_i^\phi}{\partial x} \frac{\partial \Gamma_j^\psi}{\partial x} - d_{33} \frac{\partial \Gamma_i^\phi}{\partial z} \frac{\partial \Gamma_j^\psi}{\partial z} \right] \mathrm{d}V, \tag{61}$$

$$K_{ij}^{\psi\psi} = \int_V \left[-\mu_{11} \frac{\partial \Gamma_i^\psi}{\partial x} \frac{\partial \Gamma_j^\psi}{\partial x} - \mu_{33} \frac{\partial \Gamma_i^\psi}{\partial z} \frac{\partial \Gamma_j^\psi}{\partial z} \right] \mathrm{d}V. \tag{62}$$

References

[1] C.K. Lee, Piezoelectric Laminates for Torsional and Bending Control: Theory and Experiments, PhD Dissertation, Cornell University, Ithaca, New York, 1987.

[2] C.K. Lee, F.C. Moon, Laminated piezopolymer plates for torsion and bending sensing and actuators, *Journal of the Acoustical Society of America* 85 (1989) 2432–2439.

[3] C.K. Lee, Theory of laminated piezoelectric plates for the design of distributed sensors/actuators, Part I: governing equations and reciprocal relationships, *Journal of the Acoustical Society of America* 87 (1990) 1144–1158.

[4] C.K. Lee, F.C. Moon, Modal sensors/actuators, *ASME Journal of Applied Mechanics* 57 (1990) 434–441.

[5] H.S. Tzou, M. Gadre, Theoretical analysis of a multi-layered thin shell actuators for distributed vibration controls, *ASME Journal of Sound and Vibration* 132 (1989) 433–450.

[6] P.R. Heyliger, Static behavior of laminated elastic/piezoelectric plates, *AIAA Journal* 32 (1994) 2481–2484.

[7] P.R. Heyliger, S. Brooks, Exact solutions for laminated piezoelectric plates in cylindrical bending, *ASME Journal of Applied Mechanics* 63 (1996) 903–910.

[8] P.R. Heyliger, S. Brooks, Free vibration of piezoelectric laminates in cylindrical bending, *International Journal of Solid and Structures* 32 (20) (1995) 1960–2945.

[9] G. Harshe, J.P. Dougherty, R.E. Newnham, Theoretical modeling of multilayer magnetoelectric composites, *International Journal of Applied Electromagnetics* 4 (1993) 145–159.

[10] C.W. Nan, Magnetoelectric effect in composites of piezoelectric and piezomagnetic phases, *Physics Review B* 50 (1994) 6082–6088.

[11] Y. Benviste, Magnetoelectric effect in fibrous composites with piezoelectric and piezomagnetic phases, *Physics Review B* 51 (1995) 16424–16427.

[12] E. Pan, Exact solution for simply supported and multilayered magneto-electro-elastic plates, *Journal of Applied Mechanics* 68 (2001) 608–618.

[13] E. Pan, P.R. Heyliger, Exact solutions for magnetoelectroelastic laminates in cylindrical bending, *International Journal of Solids and Structures* 40 (2003) 6859–6876.
[14] E. Pan, P.R. Heyliger, Free vibration of simply-supported and multilayered magneto-electro-elastic plates, *Journal of Sound and Vibration* 252 (2002) 429–442.
[15] P.R. Heyliger, E. Pan, Static fields in magnetoelectroelastic laminates, *AIAA Journal* 42 (7) (2004).
[16] P.R. Heyliger, F. Ramirez, E. Pan, Two-dimensional static fields in magneto-electroelastic laminates, *Journal of Intelligent Material Systems and Structures* 15 (9–10) (2004) 689–709.
[17] A.M. Jiang, H.J. Ding, Analytical solutions to magneto-electro-elastic beams, *Structural Engineering and Mechanics* 18 (2) (2004) 195–209.
[18] R.G. Lage, C.M.M. Soares, C.A.M. Soares, J.N. Reddy, Layerwise partial mixed finite element analysis of magneto-electro-elastic plates, *Computer & Structures* 82 (17–19) (2004) 1293–1301.
[19] G.R. Buchanan, Layered versus multiphase magneto-electro-elastic composites, *Composites Part B—Engineering* 35 (5) (2004) 413–420.
[20] S. Latheswary, K.V. Valsarajan, Y.V.K.S. Rao, Dynamic response of moderately thick composite plates, *Journal of Sound and Vibration* 270 (1–2) (2004) 417–426.
[21] S.S. Vel, R. Mewer, R.C. Batra, Analytical solution for the cylindrical bending vibration of piezoelectric composite plates, *International Journal of Solids and Structures* 41 (2004) 1625–1643.
[22] D.A. Berlincourt, D.R. Curran, H. Jaffe, *Physical Acoustics*, *1*: *Piezoelectric and Piezomagnetical Materials and their Function in Transducers*, 1964, pp. 169–270.
[23] J.N. Reddy, *Energy and Variational Methods in Applied Mechanics*, Wiley, New York, 1984.
[24] J.N. Reddy, A generalization of displacement-based laminate theories, *Communications in Applied Numerical Methods* 3 (1987) 173–181.
[25] P.R. Heyliger, Exact solutions for simply-supported laminated piezoelectric plates, *Journal of Applied Mechanics* 64 (1997) 299–306.
[26] *ABAQUS User's Manual*, Version 6.1, Hibbit, Karlsson & Sorensen, 2000.